ADVANCED HEALTHCARE MATERIALS
www.advhealthmat.de

High-Resolution Projection Microstereolithography for Patterning of Neovasculature

*Ritu Raman, Basanta Bhaduri, Mustafa Mir, Artem Shkumatov, Min Kyung Lee, Gabriel Popescu, Hyunjoon Kong, and Rashid Bashir**

To gain a quantitative understanding of the way cells sense, process, and respond to dynamic environmental signals in real-time requires developing in vitro model systems that accurately replicate the 3D structure and function of native tissue. A high-resolution projection stereolithography apparatus (μSLA) capable of multimaterial and grayscale 3D patterning of cells and biomaterials at <5 μm resolution is presented. Murine cells (fibroblasts, myoblasts, endothelial, and bone marrow stromal cells) encapsulated within photosensitive hydrogels using the μSLA remain viable up to two weeks after fabrication. Harnessing the high-resolution fabrication capabilities of this machine, sub-millimeter scale angiogenic cell-encapsulating patches designed to promote targeted growth of neovasculature are printed, as assessed in vitro via enzyme-linked immunosorbent assay (ELISA) and in ovo via a chick chorioallantoic membrane assay (CAM). This application establishes the μSLA as an enabling technology that is widely adaptable to any application that requires high-resolution patterning of cells and cells signals. By providing an efficient and robust method of engineering microscale tissues with encapsulated cells, this apparatus has a range of applications including fundamental studies of extracellular matrix interactions, high throughput drug testing of physiologically relevant substitutes for native tissue, and programmable tissue engineering for applications in regenerative medicine.

1. Introduction

Cells in their native environment are arranged in precise 3D architectures that promote cell–cell and cell–matrix interactions.[1] A complex range of dynamic biological, chemical, electrical, and mechanical signals from the surrounding microenvironment control cellular function.[2] To gain a quantitative understanding of the way cells sense, process, and respond to dynamic environmental signals in real-time, we need to develop in vitro model systems that accurately replicate the 3D structure and function of native tissue. Such models have a range of applications including fundamental studies of extracellular matrix interactions, high throughput drug testing of physiologically relevant substitutes for native tissue, and programmable tissue engineering for applications in regenerative medicine.[3–7]

Recent efforts to replicate the in vivo cellular environment in an in vitro setting have harnessed the ability of additive manufacturing, or "3D printing," apparatus to pattern cells in complex architectures.[8,9] Stereolithography, a subtype of additive manufacturing, was the first commercially available 3D printing technology and is widely used in a variety of industry sectors due to its efficiency, versatility, and superior quality of fabricated parts.[10] The mass commercial adaptation of stereolithography apparatus (SLA) technologies, combined with increasing availability of biocompatible, bioactive, and biodegradable photosensitive resins, has led to widespread adaptation of SLA for biomedical engineering applications.[11,12]

Conventional stereolithography relies on the use of ultraviolet light to selectively polymerize photosensitive materials

R. Raman
Department of Mechanical Science and Engineering
Micro and Nanotechnology Laboratory
University of Illinois at Urbana-Champaign
Urbana, IL 61801, USA

Dr. B. Bhaduri, Prof. G. Popescu
Department of Electrical and Computer Engineering
Beckman Institute for Advanced Science
University of Illinois at Urbana-Champaign
Urbana, IL 61801, USA

Dr. M. Mir
Department of Molecular and Cell Biology
University of California
Berkeley, Berkeley, CA 94720, USA

DOI: 10.1002/adhm.201500721

Dr. A. Shkumatov
Department of Pathobiology
Carl R. Woese Institute for Genomic Biology
University of Illinois at Urbana-Champaign
Urbana, IL 61801, USA

Dr. M. K. Lee, Prof. H. Kong
Department of Chemical and Biomolecular Engineering
Carl R. Woese Institute for Genomic Biology
University of Illinois at Urbana-Champaign
Urbana, IL 61801, USA

Prof. R. Bashir
Department of Bioengineering and Electrical and Computer Engineering
Micro and Nanotechnology Laboratory
University of Illinois at Urbana-Champaign
Urbana, IL 61801, USA
E-mail: rbashir@illinois.edu

into complex 3D architectures. Most commercially available SLA manufacture parts by using a UV laser to sequentially trace 2D cross-sections of a 3D model. Parts are thus sequentially built layer by layer from the bottom up. Projection stereolithography offers a variation on this traditional method. Rather than tracing of 2D cross-sections, these apparatus project UV light through a mask, polymerizing entire cross-sections in a single exposure. While the first projection SLA machines utilized physical masks,[13–15] these were soon replaced by dynamic digital masks that allowed for high-resolution and high-throughput patterning and fabrication of a myriad array of 3D architectures.[16,17]

At the forefront of 3D bioprinting is the fabrication of 3D structures with encapsulated cells, which has been demonstrated using both laser-based and projection SLA.[18–21] Engineering in vitro model systems that recreate the structure and function of native tissue requires the ability to pattern cells and cell signals at physiologically relevant length scales (1–50 µm).[22] There have been limited reports on projection SLA-based cellular patterning at length scales <50 µm,[21] but no demonstrations of patterning at resolutions <10 µm, the diameter of single cells. Furthermore, there has been no reported assessment of long-term cellular viability following the projection SLA fabrication process, and no demonstration of practical applications for such a technology.

Here we present a custom-built projection SLA apparatus (µSLA) capable of patterning features at <5 µm resolution using a biocompatible hydrogel resin. We demonstrate multimaterial fabrication of complex structures in 3D, and a novel method of building 3D objects with smooth features in a single exposure using a grayscale digital mask. Long-term viability of multiple cell types encapsulated within different hydrogel compositions using the µSLA is demonstrated, proving the applicability of this technology for a wide variety of applications in biomedical engineering. To specifically target an application of this technology in vascularization, we use the µSLA to fabricate angiogenic "patches" that encapsulate cells capable of endogenously secreting a series of proangiogenic cytokines and growth factors. Following design optimization of the angiogenic patches via enzyme-linked immunosorbent assay (ELISA) assay, the patches are tested in a chick chorioallantoic membrane (CAM) model and proven to encourage the formation of neovasculature in ovo. This sets the stage for future work in printing angiogenic patches with microscale feature sizes for therapeutic applications in treating tissue ischemia and defects in vivo. As the first demonstration of gray-scale fabrication, long-term cellular viability, and a practical application of a projection SLA, this study establishes projection microstereolithography as a promising enabling tool for a wide variety of applications in biomedical engineering.

2. Results and Discussion

2.1. High-Resolution 3D Fabrication

A high-resolution µSLA was designed and custom-built around a spatial light modulator (SLM) extracted from a commercial digital multimedia projector (**Figure 1**A). For ease of implementation, the SLM, which acts as a dynamic mask for polymerization, was integrated in the optical path while remaining connected to the projector through an extended cable. As a result, the projector can simply be connected to a computer as in regular use, and images on the computer screen are reproduced as grayscale pixelated images on the SLM. This enables dynamic 2D patterning of light projected through the digital mask. UV light (365 nm) is collimated and projected through the SLM and the resulting image is demagnified through a 10× microscope objective (NA = 0.3) onto the polymerization plane. Prepolymer solution is rendered photosensitive via the addition of a biocompatible photoinitiator (Irgacure 2959) known to react to light at this wavelength.[23,24] This solution is then dispensed in controlled volumes at the polymerization plane, forming 2D hydrogel patterns in response to patterned UV light exposure. Illuminated regions form cross-linked hydrogel networks, whereas nonilluminated regions do not polymerize.

2.1.1. Fabrication Resolution for Hydrogel Resins

Among the most promising photosensitive polymer resins for SLA are hydrogels, highly hydrophilic materials formed from chemical or physical cross-linking of monomers.[25] Synthetic hydrogels can be readily tuned to have well defined biochemical and mechanical properties, rendering them an attractive biomaterial for biomedical engineering applications.[26] Specifically, synthetic poly(ethylene glycol) (PEG) based hydrogels, sometimes modified with integrin-binding peptides and proteins, have been widely used due to their ability to viably encapsulate living cells and sustain proliferation in vitro.[27]

The challenge of fabricating high-resolution features with PEG-based hydrogel resins arises from the swelling behavior of these incredibly absorbent materials. With increasing molecular weight of the base monomer, the porosity and swelling of the cross-linked network increases. As a result, cells demonstrate greater viability in hydrogel networks with base monomers of higher molecular weight, as the increased porosity allows for enhanced diffusion of nutrients from the surrounding media into the cross-linked 3D structure.[18] Figure 1B-1 demonstrates fabrication with a poly(ethylene glycol) dimethacrylate (PEG-dma) resin of molecular weight (M_w) 1000 g mol^{-1}. A pattern of lines and holes of decreasing size is polymerized, demonstrating that feature sizes down to 3 µm (in a 100 µm thick hydrogel) can be fabricated using the µSLA. A resin of higher molecular weight, namely, poly(ethylene glycol) diacrylate (PEG-da) of M_w 3400 g mol^{-1}, was also tested for fabrication resolution. Patterns of lines and holes down to 30 µm were fabricated using the µSLA (Figure S1-A, Supporting Information). This increase in minimum feature size is attributed to the larger swelling ratios of cross-linked hydrogel networks composed of longer chain monomers.

The incorporation of additional materials (such as cells, colored dyes, etc.) into the prepolymer solution can cause dispersion of the projected UV light, resulting in a reduced ability to resolve small features. However, at moderate cell concentrations ranging from 5×10^6 to 1×10^7 cells mL^{-1}, fabrication resolution is not compromised (Figure 1B-2). Cells mixed within

Adv. Healthcare Mater. 2015,
DOI: 10.1002/adhm.201500721

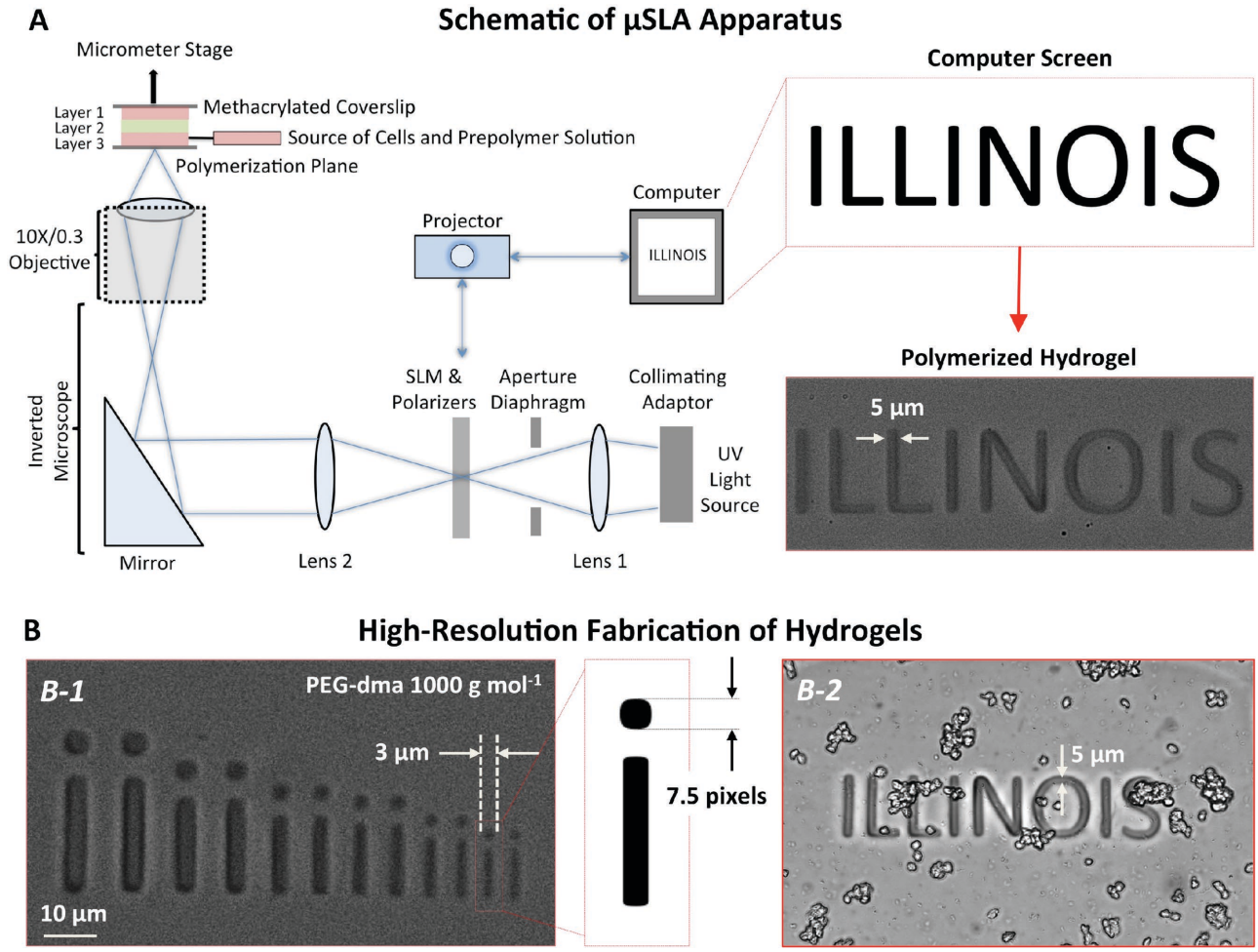

Figure 1. μSLA setup and high resolution fabrication demonstration. A) Schematic of μSLA showing UV light collimated and projected through a spatial light modulator that acts as a dynamic mask for polymerization. Patterned UV light is demagnified through a microscope objective and focused onto the polymerization stage, where it selectively cross-links photosensitive resins. 3D parts are built layer by layer from the bottom up in an upside down orientation (Figure S2B, Supporting Information). B) High resolution fabrication of biocompatible hydrogels. B-1) Fabrication with PEG-dma 1000 g mol^{-1} at <5 μm *x*–*y* resolution. B-2) Polymerization with PEG-dma 1000 g mol^{-1} containing encapsulated cells (at a concentration 5E6 cells mL^{-1}) does not compromise high-resolution fabrication capabilities.

the prepolymer solution are encapsulated in the cross-linked hydrogel network during polymerization. Diffusion of nutrients from surrounding media is enabled by the porous nature of the 3D hydrogels of both molecular weights 1000 and 3400 g mol^{-1}.

2.1.2. Multimaterial 3D Fabrication

The thickness of a polymerized hydrogel is dictated by the degree of UV-mediated cross-linking, as predicted by an adapted form of the Beer–Lambert equation which relates the intensity of a light source to its penetration depth within a resin.[28] Regulating the energy dose of UV light, which is a function of both light source power and exposure time, thereby provides a precise method of fabricating 3D structures of specified layer thicknesses. Figure S1-B (Supporting Information) shows the relationship between energy dose and thickness for both 1000 and 3400 g mol^{-1} PEG-based resins. The lines fitted to these data were used to fabricate 3D structures of precisely dictated layer thickness.

To enable fabrication of multilayer structures, the prepolymer solution was injected onto the hydrophobic polymerization plane and covered by a glass coverslip connected to a micrometer stage. The surface of this coverslip was chemically modified to present methacrylate functional groups which cross-linked with the prepolymer resin during UV exposure and patterning. Following the polymerization of the first layer of a 3D part, the micrometer stage moved up, and the chemically tethered first layer moved up with the stage. This allowed for the injection of more resin onto the polymerization plane and cross-linking of the second layer. In this manner, 3D structures were polymerized layer-by-layer from the bottom-up (Movie S1, Supporting Information).

One of the disadvantages of both laser-based and projection SLA has been the difficulty of fabricating multimaterial structures. In prior studies, researchers have accomplished multimaterial fabrication with SLA by incorporating multiple wash steps between fabricated layers,[18,29] or modifying the fabrication platform through the addition of mini "vats" containing

different polymers.[30] A simple design modification allowed us to simplify the process of building multimaterial 3D structures, thereby increasing fabrication efficiency. Most previously presented projection SLA systems build parts layer by layer from the bottom-up, as does the μSLA presented here.[17,29,31] However, while these apparatus build parts in the "right-side-up" orientation (Figure S2A, Supporting Information), where the stage moved down for each polymerized layer, our system builds parts "upside down," or inverted (Figure S2B, Supporting Information). This modification removes each fabricated layer from the surrounding resin, rather than submerging it deeper within, thus eliminating the need for a wash step. Furthermore, the next layer of prepolymer can be directly injected onto the polymerization stage, without requiring the removal of the stage. This allows for a significant increase in fabrication efficiency. When fabricating with cells encapsulated within a polymer, the traditional "right-side-up" orientation comes with the disadvantage of cells settling to the bottom of the stage during polymerization. With our inverted fabrication setup, cells in each layer are thoroughly mixed and polymerized before settling, enabling 3D uniformity in cell-laden hydrogels (Figure S3, Supporting Information).

The μSLA's ability to fabricate parts with high-resolution feature sizes is maintained while fabricating 3D multilayer and multimaterial structures. A demonstration of negative features (i.e., holes/channels) in a two-layer dual material structure is presented in **Figure 2**A-1. This 3D design is fabricated by first polymerizing a uniform rectangle using a pink-dyed PEG-dma 1000 g mol^{-1} resin followed by polymerization of a cross-hatch pattern using a clear PEG-dma 1000 g mol^{-1} resin. As observed in top view and side view images taken 1 h postfabrication, 5 μm wide channels are formed in the second layer. Similarly, Figure 2A-2 presents fabrication of positive features (concentric cylinders of decreasing diameter) in a two-layer dual material structure.

Multimaterial 3D fabrication is also demonstrated with encapsulated NIH/3T3 fibroblast cells (Figure 2B). Unlike the structures presented in Figure 2A, in which the resin itself was dyed, the cells encapsulated in each layer of this dual-layer structure are stained with long-term live cell fluorescent stains (Layer 1—Green, Layer 2—Red) and encapsulated within a clear PEG-da 3400 g mol^{-1} resin. The fluorescent image, taken 24 h postfabrication, shows that the stained cells are segregated in each layer, with some cells crossing the boundary between layers due to proliferation and migration over the 24 h incubation. This demonstration sets the stage for fabricating multimaterial 3D structures composed of multiple cell types, a capability that is fundamental to developing tissue/organ mimics in vitro for applications in tissue engineering and organ-on-a-chip devices.

2.1.3. Grayscale Fabrication

Most projection stereolithography apparatus employ digital micromirror devices (DMD) as dynamic masks for polymerization.[17,32] These devices, which rely on moving

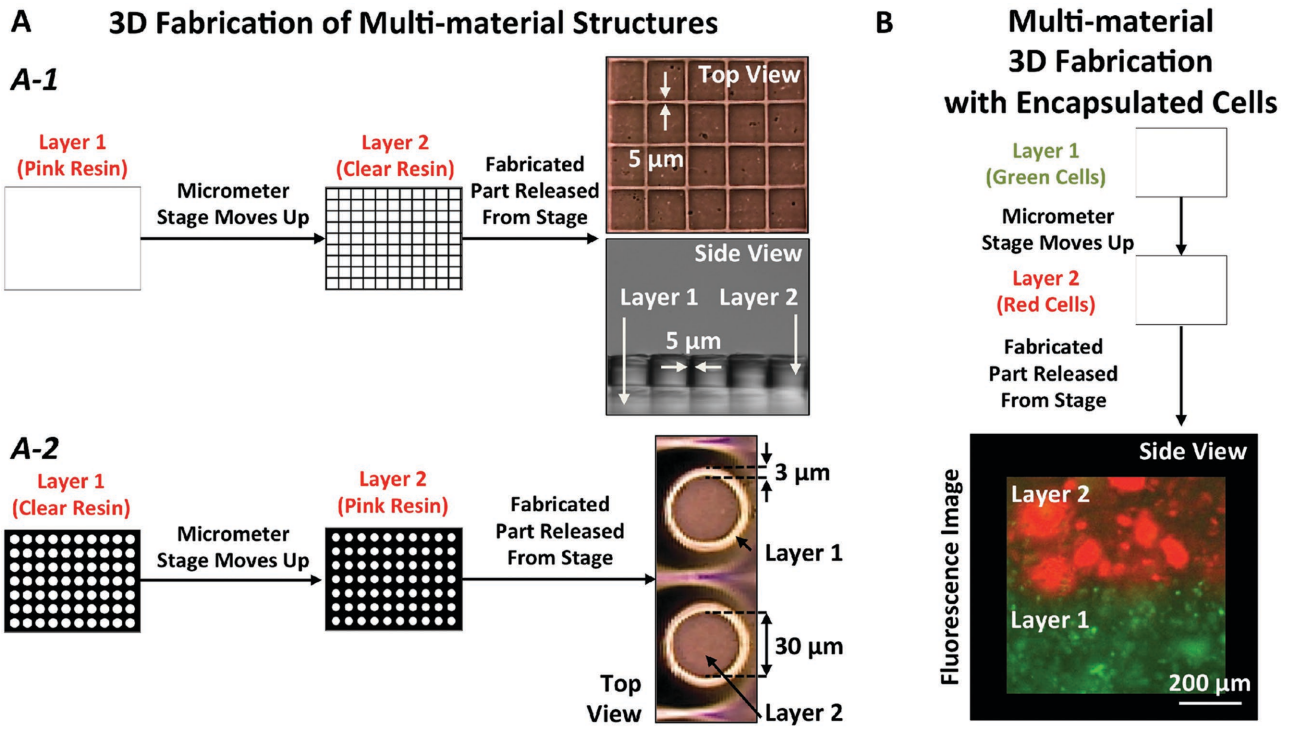

Figure 2. Multimaterial 3D fabrication with μSLA. A) Multimaterial fabrication of 3D structures is demonstrated with both "negative" features A-1) and positive features A-2). Parts are fabricated by projecting UV light in the pattern and onto the resin prescribed as Layer 1. The micrometer stage then moves up 75 μm and the second layer is fabricated with the resin and UV light pattern labeled Layer 2. The fabricated part is then released from the stage. B) Multimaterial fabrication of 3D structures containing encapsulated cells. Layer 1 contains cells stained with a green fluorescent dye and Layer 2 contains cells stained with a red fluorescent dye. Image taken 24 h after fabrication.

Adv. Healthcare Mater. **2015**,
DOI: 10.1002/adhm.201500721

microscale metal mirrors to turn pixels "on" and "off," can be reliably used to reproduce black and white images. Grayscale fabrication with digital masks that produce three grayscale levels (black, white, and gray) have also been demonstrated with projection SLA, with applications in creating self-sacrificial structures that are chemically etched to produce overhanging features.[33] Building on this demonstration, the SLM used in the μSLA system presented here is one of the three chips from a multimedia projector (Epson Powerlite S5) which is capable of producing multilevel (eight-bit) grayscale images. Since the thickness of a hydrogel structure is dictated by the degree of exposure to UV light, this grayscale projection enables the fabrication of smooth 3D structures in a single exposure. For example, fabricating a simple dome-shaped 3D structure with a DMD-based SLA would require sequential exposure of multiple circular layers, each with decreasing diameter. This gives the dome a rough ladder-like surface, with surface roughness dictated by layer thickness (Figure S4A, Supporting Information). Using the SLM-based μSLA, however, this dome-shaped structure can be fabricated in one step by projecting a grayscale 2D image with light intensity decreasing radially from the center (**Figure 3**A1–2 and Figure S4B, Supporting Information). Processing these images in 3D and plotting the relative intensity along a line drawn across the dome show that the height of different regions in the fabricated part is dictated by the corresponding intensity of projected light at that region (Figure 3A3). A similar demonstration of a negative feature (dome-shaped hole) shows that grayscale-enabled fabrication of smooth features is applicable to a variety of 3D part designs (Figure 3B).

2.2. Cell Viability

There have been limited reports of cellular viability postencapsulation using a projection stereolithography apparatus,[21] and no demonstrations of viability in multiple cell types over a long-term in vitro culture period (more than a week). Establishing projection SLA as an enabling tool for applications in tissue engineering thus requires definitive proof of cellular viability and maintenance of cellular function following the printing process. In this study, we mixed murine cells of four types (C2C12 myoblasts, C166 endothelial cells, NIH/3T3 fibroblasts, and D1 bone marrow stromal cells) with prepolymer PEG-dma 1000 g mol^{-1} and PEG-da 3400 g mol^{-1} resins. Rectangular hydrogel blocks (740 μm × 530 μm wide, 360 μm thick) containing cells encapsulated at 7.5×10^6 cells mL^{-1} concentration (corresponding to ≈1000 cells/hydrogel block) were fabricated for each cell type and each hydrogel resin. Viability of cells seeded within these blocks was quantitatively assessed via MTS (3-(4,5-dimethylthiazol-2-yl)-5-(3-carboxymethoxyphenyl)-2-(4-sulfo-phenyl)-2H-tetrazolium)) colorimetric assay, which measures the absorbance of a purple formazan byproduct that indicates the presence of metabolically active cells (**Figure 4**A). The MTS assay was performed on the day after fabrication (day 1),

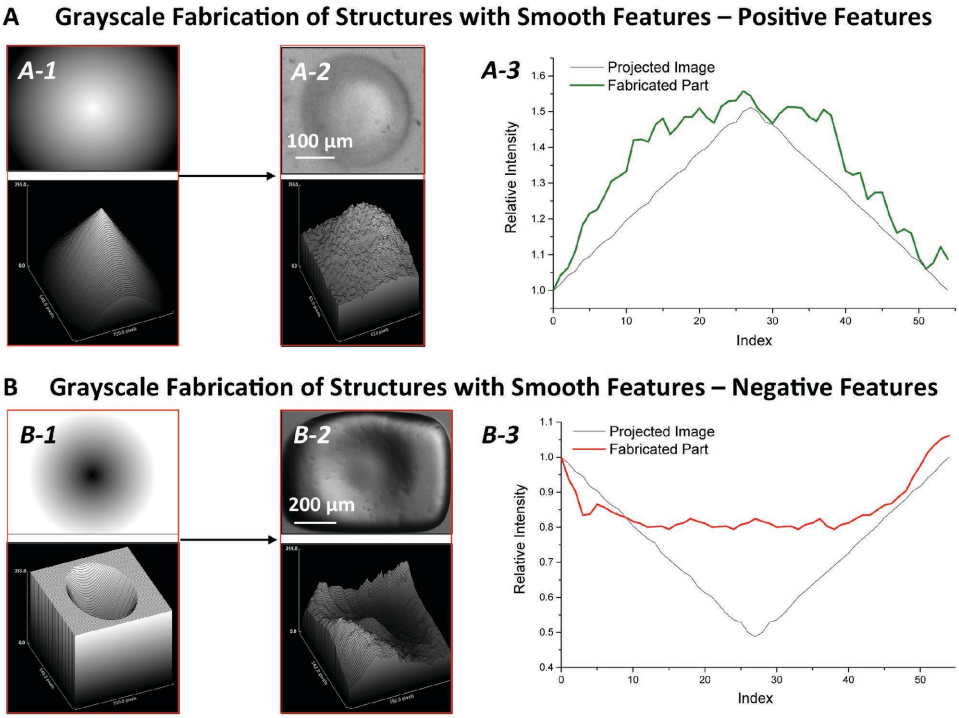

Figure 3. Grayscale fabrication of structures. A) A grayscale projected image (A-1, top) produces a smooth dome-like structure (A-2, top) in a single exposure. 3D projection of light intensity is shown for both the projected image (A-1, bottom) and the fabricated part (A-2, bottom). A-3) Graph showing the relative light intensity of both the projected image and the fabricated part along a line drawn across both images. B) A grayscale projected image (B-1, top) produces a smooth dome-like hole (B-2, top) in a single exposure. 3D projection of light intensity is shown for both the projected image (B-1, bottom) and the fabricated part (B-2, bottom). B-3) Graph showing the relative light intensity of both the projected image and the fabricated part along a line drawn across both images.

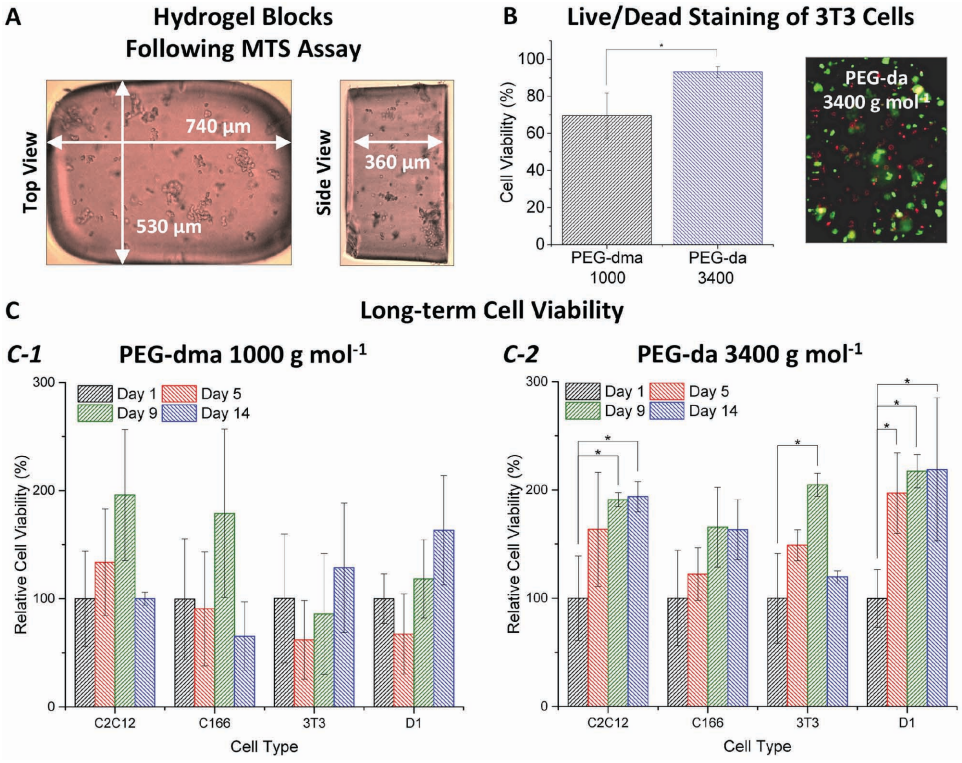

Figure 4. Long-term viability of printed cells. A) Hydrogel blocks imaged after an MTS assay used to quantify cell viability. The formation of purple formazan crystals indicates the presence of living cells. B) Live/dead staining of 3T3 fibroblast cells encapsulated in hydrogel PEG-based resins of M_w 1000 and 3400 g mol^{-1}. Cells encapsulated in the lower molecular weight polymer demonstrate a viability of 70% ± 10%, whereas cells encapsulated in the higher molecular weight polymer (representative live/dead stained fluorescent image shown on right) demonstrate a viability of 93% ± 3% on day 1 after printing ($P < 0.05$, $n = 4$, one-way analysis of variance (ANOVA), post hoc Tukey test). C) Cell viability over a two week period is assessed via MTS assay for four cell types (C2C12 myoblasts, C166 endothelial cells, 3T3 fibroblasts, and D1 bone marrow stromal cells) for PEG-based resins of M_w 1000 C-1) and 3400 g mol^{-1} C-2) ($P < 0.05$, $n = 3$, one-way ANOVA, post hoc Tukey test). Viability is shown relative to viability on day 1 (i.e., all MTS absorbance values are normalized to the absorbance on day 1). For all cell types in PEG-dma M_w 1000 g mol^{-1}, viability does not significantly change over the two week period. For all cell types in PEG-da M_w 3400 g mol^{-1}, viability increases over the two week period, with significant increases observed in C2C12, 3T3, and D1 cells.

to establish a baseline on cell viability. Relative cell viabilities on days 5, 9, and 14 were then calculated by normalizing the measured absorbance on each day with the absorbance measured on day 1. The actual viability (specified by the number of live cells divided by the total number of encapsulated cells) for each resin formulation was calculated via live/dead fluorescent staining. These viability results, which show statistically significant improvements in viability for PEG-da 3400 g mol^{-1} as compared to PEG-dma 1000 g mol^{-1}, are presented for NIH/3T3 cells but were consistent across the four cell types (Figure 4B).

For PEG-dma M_w 1000 g mol^{-1}, viability was calculated via live/dead staining to be 70% ± 10% on day 1 following fabrication. The viability of all four cell types demonstrated neither significant increase nor decrease over the two-week culture period, proving that cellular viability was maintained in this resin following encapsulation via the µSLA (Figure 4C-1). For PEG-da M_w 3400 g mol^{-1}, viability was calculated to be 93% ± 3% on day 1 following fabrication. The relative cell viability, as calculated via the MTS assay, increased for all cell types over the two-week culture period, with statistically significant increases seen for C2C12, 3T3, and D1 cell types (Figure 4C-2). The enhanced viability in PEG-da M_w 3400 g mol^{-1} as compared to PEG-dma M_w 1000 g mol^{-1} is attributed to the larger pore sizes present in hydrogel networks composed of higher molecular weight (i.e., longer-chain) monomers.[18] While the increased swelling ratio of this resin postcrosslinking limits the highest observable resolution in fabricated parts (30 µm for PEG-da M_w 3400 g mol^{-1} vs 3 µm for PEG-dma M_w 1000 g mol^{-1}), the corresponding increase in diffusion of nutrients from surrounding media motivates the use of M_w 3400 g mol^{-1} in biomedical applications that require maximum cellular viability.

2.3. Patterning of Neovasculature

Trauma or disease that results in the reduction of blood supply to tissue in vivo produces ischemia, which can severely damage surrounding tissue.[34] Current treatment for ischemia relies largely on the use of anticoagulants, but recent developments in regenerative medicine motivate therapeutic treatment of ischemia by an alternative method: encouraging the formation of neovasculature to renew blood supply to the damaged tissue.[35] Prior studies have demonstrated that targeted secretion of angiogenic factors, such as vascular endothelial growth factor (VEGF) and endothelin, from cell-encapsulating hydrogel patches can drive the formation of new blood vessels on a chick

Adv. Healthcare Mater. 2015,
DOI: 10.1002/adhm.201500721

chorioallantoic membrane in ovo model.[36] The incorporation of channels hundreds of micrometers wide within these centimeter-scale patches enhanced the flux of cell-secreted VEGF onto the CAM. This micropatterned release of biomolecules into tissue helped guide the growth direction and spacing of new blood vessels. This demonstration was sufficiently successful as a first demonstration, but true applicability as an in vivo therapy requires that such angiogenic patches be scaled down to the submillimeter length scale to allow for noninvasive injection into tissue via catheters. This scale reduction would increase the viability of cells encapsulated within the angiogenic patches, and the incorporation of smaller channels within these patches would increase the diffusive flux of VEGF from patch to tissue. This design challenge can readily be addressed by the high-resolution fabrication capabilities of the μSLA.

2.3.1. Analysis of VEGF Secretion In Vitro Via ELISA

Two angiogenic patch designs were assessed for VEGF secretion via ELISA: (1) a "plain patch" consisting of a simple hydrogel block (740 μm × 530 μm wide, 360 μm thick) and (2) a "microchanneled patch" consisting of a hydrogel block (740 μm × 530 μm wide, 360 μm thick with four 100 μm diameter channels). Both types of patches encapsulated ≈900 NIH/3T3 fibroblast cells activated to release proangiogenic factors. These channels were expected to increase the diffusive flux of VEGF out of the patches and into the surrounding medium by enhancing the ratio of surface area/volume (**Figure 5**A). Furthermore, by reducing the distance between any encapsulated cell and the surrounding medium, the microchanneled design enhanced diffusion of nutrients from the surrounding medium into the patches. To test the hypothesis that microchanneled patches would enhance the diffusive flux of cell-secreted VEGF, we fabricated patches of each design and incubated them in warm growth medium containing tetradecanoylphorbol 13-acetate (TPA), a chemical known to stimulate cells to secrete VEGF.[36] Optical density of the fluorescent signal produced during the ELISA test (performed after 3 d of incubation) was measured for both patch designs, as well as for a negative control (growth medium containing TPA, no patches or cells) and a positive control (cells seeded in a well containing growth medium supplemented with TPA) (Figure S5A, Supporting Information). Optical density was converted to an actual concentration using a calibration curve (Figure S5B, Supporting Information). Microchanneled patches produced 136.1 ± 4.8 ng mL^{-1} VEGF, significantly greater than the amount produced by plain patches of 72.4 ± 27 ng mL^{-1} VEGF (Figure 5B). As expected, no VEGF was detected in the negative control. Both plain and microchanneled patches produced greater amounts of VEGF than the positive control. This was explained by the observation that cells were migrating out of the patches and proliferating on the base of the wells, contributing to the increased VEGF production observed via ELISA. Based on these results, microchanneled patches were used in subsequent CAM assay experiments.

2.3.2. Analysis of VEGF Secretion In Ovo Via CAM Assay

To test the efficacy of the microchanneled patches in producing VEGF and encouraging vascular regeneration in an in ovo setting, we fabricated microchanneled patches with encapsulated NIH/3T3 fibroblasts, incubated them in growth medium containing TPA for 1 d, and then placed them onto a chick chorioallantoic membrane for one week (**Figure 6**A). The membranes were then sectioned and stained for DAPI (4′6-diamidino-2-phenylindole) (cell nuclei) and smooth actin (Figure 6B). The number of blood vessels and the areas of blood vessels were quantified in a control group and a test group by imaging histological cross-sections. The control group membranes were incubated with "unloaded" microchanneled patches that did not contain encapsulated cells, and the test group membranes were incubated with "loaded" microchanneled patches containing encapsulated and TPA-stimulated NIH/3T3 fibroblasts. After one week, the membranes incubated with loaded patches had 12.1% ± 1.1% vessel area/tissue area, whereas membranes incubated with unloaded patches had a significantly lower percentage of 6.3% ± 0.6% vessel area/tissue area (Figure 6C-1). These results indicate that the loaded microchanneled patches were indeed angiogenic and encouraged the formation of

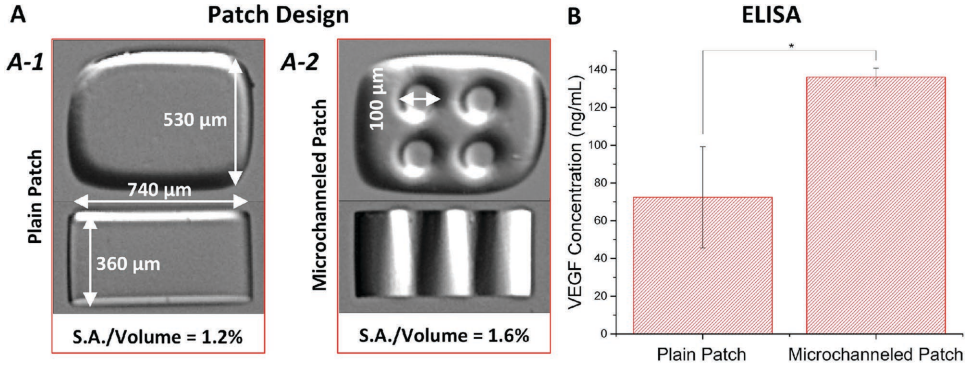

Figure 5. Angiogenic patch design verification. A) Patch design and dimensions shown (without encapsulated cells) for both the plain patch A-1) and microchanneled patch A-2) designs. Plain patches had a calculated surface area to volume ratio of 1.2% and microchanneled patches had a calculated surface area to volume ratio of 1.6%. B) VEGF secretion assessed via ELISA. Using the calibration curve and fitted equation shown in Figure S5B (Supporting Information), optical density values (Figure S5A, Supporting Information) are converted to concentrations of secreted VEGF for plain patches and microchanneled patches. Microchanneled patches produced significantly higher concentrations of secreted VEGF than plain patches ($P < 0.05$, $n = 3$, one-way ANOVA, post hoc Tukey test).

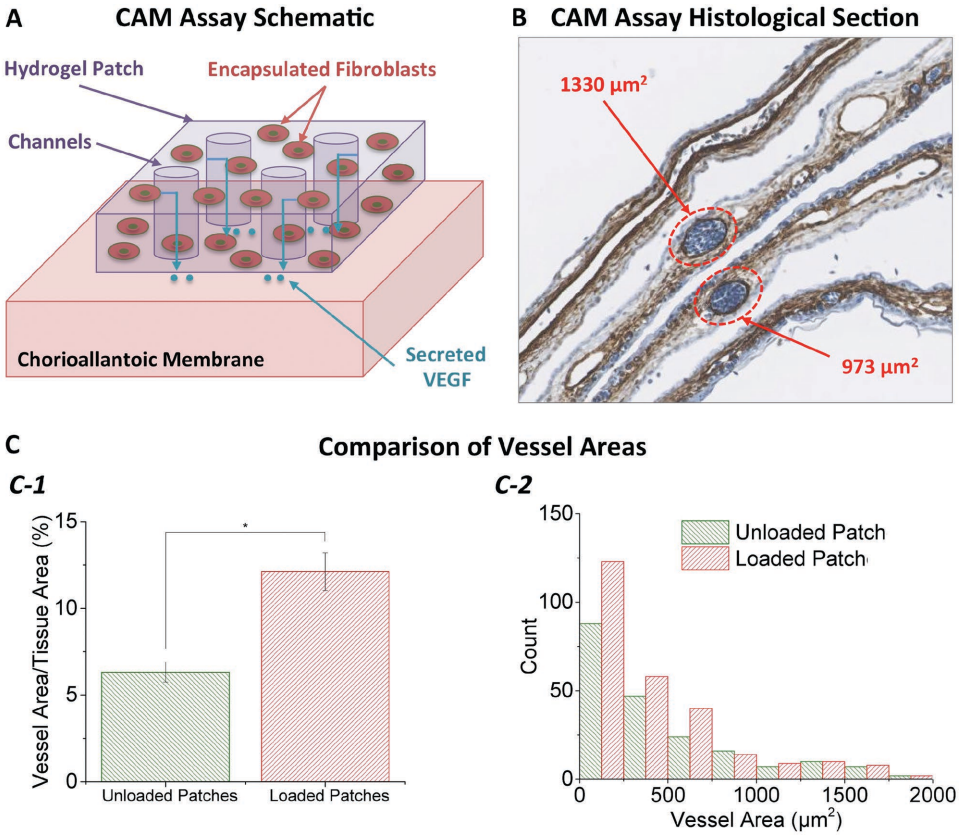

Figure 6. Angiogenic functionality of patches assessed via CAM assay. A) Schematic of CAM assay showing a microchanneled patch containing encapsulated fibroblasts placed on a chick chorioallantoic membrane. The encapsulated cells are TPA-stimulated to secrete VEGF, encouraging the formation of neovasculature on the CAM. B) A histological section of the CAM assay, stained for cell nuclei stain (haematoxylin, blue) and alpha-smooth actin (brown), is used to quantify the number of blood vessels as well as the area of blood vessels within the membrane. Two vessels are specifically highlighted to show how areas were measured. C) Comparison of vessel areas in the control (unloaded patches) and loaded patches groups. Patches loaded with VEGF-secreting fibroblasts had a greater percentage of vessel area/tissue area C-1) than the control ($P < 0.05$, $n = 3$, one-way ANOVA, post hoc Tukey test). The vessel areas were widely distributed in both experimental groups C-2), with an increased number of vessels observed in loaded patches as compared to the control.

neovasculature in ovo. A histogram displaying the distribution of blood vessel area for a representative sample from the unloaded and loaded patch groups shows the broad variation in vessel size for both groups (Figure 6C-2). Loaded patches had, on average, 133 vessels mm^{-2} tissue area and unloaded patches had, on average, 54 vessels mm^{-2} tissue area. Hence it is evident that the loaded patches enhanced angiogenesis in the membrane by stimulating the growth of new blood vessels.

3. Conclusion

Adaptation of 3D printing technologies to biofabrication has recently enabled many applications in biomedical engineering. While stereolithography has long been established as one of the most robust approaches for patterning cells and biomaterials in 3D, high-resolution projection SLA machines have only recently been applied to this area. As a result, very few studies have examined the use of projection SLA systems for fabricating complex 3D structures with encapsulated cells, and none to date have demonstrated multimaterial 3D patterning at resolutions <10 µm. We have demonstrated high-resolution fabrication and long-term viability of four cell types encapsulated within µSLA patterned hydrogels. The µSLA we have built is capable of multimaterial fabrication with high-resolution feature sizes in 3D and furthermore, has the ability to build smooth 3D structures in a single exposure using the grayscale capabilities of the SLM digital mask.

In this study, we exploit the high-resolution fabrication capabilities of the µSLA to address a design challenge posed by treatment of tissue ischemia via targeted angiogenesis. By fabricating submillimeter scale angiogenic patches containing VEGF-secreting cells and optimizing the design parameters via ELISA, we produced a therapeutic hydrogel patch that can be used to stimulate the growth of neovasculature in ovo as assessed via CAM assay. This demonstration sets the stage for future in vivo studies that employ a noninvasive surgical approach to treating ischemia by injecting VEGF-secreting patches via a catheter. This is anticipated to produce enhanced therapeutic outcomes as compared to traditional approaches.

While the angiogenic patches presented here represent one possible application of the µSLA technology, this machine is widely adaptable to a range of applications that require patterning of cells and cell signals at high resolution. This novel 3D printing

Adv. Healthcare Mater. 2015,
DOI: 10.1002/adhm.201500721

apparatus could be used to engineer microscale tissues and organs for high-throughput drug testing, or to study disease development in vitro. There are also myriad applications of this 3D printing machine in cell therapy and regenerative medicine for other tissue types, beyond vasculature. By providing an efficient and viable method of engineering microscale tissues with cells and cell signals patterned at resolutions on the order of single cells, this apparatus establishes itself as an enabling technology with broad applicability in the field of biomedical engineering.

4. Experimental Section

Design of μSLA Apparatus: Broadband light in the 350–650 nm wavelength range (with an intensity peak at 365 nm) from a light source (X-Cite Series 120, Lumen Dynamics) was passed through a liquid filled light guide (Lumen Dynamics). A plano-convex lens, L1 (focal length = 300.0 mm, Thorlabs), was placed after the collimating adaptor (Zeiss Axio Standard, BioVision Technologies) attached at the end of the light guide, to focus the light onto a spatial light modulator (800 × 600 pixels) sandwiched between two orthogonal polarizers (PowerLite S5, Epson). A plano convex lens, L2 (focal length = 250.0 mm, Thorlabs), acts as a tube lens prior to the objective lens (10×, NA = 0.3, WD = 16.5, Nikon). The objective was mounted in a commercial inverted microscope base (Nikon Epiphot 200) which has its internal tube lens removed and its turning mirror replaced with a UV enhanced aluminum mirror (Thorlabs). In this manner, the projection apparatus was interfaced with the microscope through its side camera port. The objective lens projects the demagnified image of the SLM pattern onto the polymerization plane. A micrometer translation stage (Thorlabs) was used to move the printed layers axially by a prescribed amount during the fabrication of 3D parts. To ensure chemical tethering of hydrogel parts to the translation stage, glass slides attached to the stage were pretreated with 2% v/v 3-trimethoxysilyl) propyl methacrylate (Sigma-Aldrich) in 100% ethanol (Decon Labs) for 5 min, washed in 100% ethanol for 5 min, and baked at 110 °C for 3 min.

Formulation of Hydrogel Resins: Hydrogel resins used for fabricating parts without encapsulated cells were composed of either 40% w/v poly(ethylene glycol) dimethacrylate M_w 1000 g mol^{-1} (PolySciences, Inc.) or poly(ethylene glycol) diacrylate M_w 3400 g mol^{-1} (Laysan Bio) in phosphate buffered saline (PBS, Lonza) with 1% w/v 1-[4-(2-hydroxyethoxy)phenyl]-2-hydroxy-2-methyl-1-propanone-1-one photoinitiator (Irgacure 2959, BASF) dissolved in dimethyl sulfoxide (Fisher Scientific). Hydrogel resins used for fabricating parts with encapsulated cells were dissolved in phenol red-free Dulbecco's modified Eagle medium (DMEM, Life Technologies) supplemented with 1% L-glutamine (Cellgro Mediatech, Inc.) and 1% penicillin–streptomycin (Cellgro Mediatech, Inc.). Murine cells (NIH/3T3 fibroblasts, C2C12 myoblasts, C166 endothelial cells, and D1 bone marrow stromal cells) were cultured in DMEM with L-glutamine and sodium pyruvate (DMEM, Corning CellGro) supplemented with 10% fetal bovine serum (FBS, Lonza), 1% L-glutamine (Cellgro Mediatech, Inc.), and 1% penicillin–streptomycin (Cellgro Mediatech, Inc.) (GM). Prior to encapsulation, they were trypsinized (TrypeLe, Life Technologies), counted, and gently resuspended in the prepolymer solution at concentrations ranging from 5E6 to 1E7 cells mL^{-1}. Fabricated parts were washed in DMEM prior to incubation at 37 °C in GM. For visualization of cells stained different colors in different layers of a 3D structure, cells were incubated with 1/1000 of green or red cell tracker (CMFDA and CMTPX Dye, Invitrogen) prior to suspension in the prepolymer solution.

Assessment of Cellular Viability: Live/dead staining of cells was conducted using a viability/cytotoxicity kit for mammalian cells (Life Technologies). Hydrogels containing encapsulated cells were incubated with calcein AM (2×10^{-6} M) and ethidium homodimer (4×10^{-6} M) for 15 min in phenol red-free DMEM (Corning CellGro), washed twice in PBS (Lonza), and imaged in an inverted fluorescence microscope. Live cells, stained green, were imaged using a FITC filter and dead cells, stained red, were imaged used a TRITC filter. ImageJ was used for counting cells from each channel and viability was calculated as the ratio of live cells to the total number of cells. Viability was quantitatively assessed over two weeks using a CellTiter 96 AQueous One Solution cell proliferation assay (MTS, Promega) by incubating hydrogels containing cells in phenol red-free DMEM (200 μL) (Life Technologies) and thawed MTS reagent (20 μL) for 4 h in the dark at 37 °C. The assay solution was then removed from the wells and absorbance (relative to a control) was measured at 490 nm using a microplate reader (BioTek). Viability relative to day 1 was calculated by first subtracting the control absorbance reading from the sample absorbance reading and then dividing by the absorbance on day 1.

Analysis of VEGF Secretion Via ELISA: NIH/3T3 cells were encapsulated within plain and microchanneled patches (≈900 cells per patch) using prepolymer solution of PEGDA M_w 3400 g mol^{-1}. Patches were incubated in wells (three patches per well) containing GM (200 μL) supplemented with 12-O-tetradecanoylphorbol-13-acetate (100 ng mL^{-1}) (TPA, Sigma-Aldrich) for 3 d. The media was then removed from the wells and frozen at –20 °C until ready for ELISA. A sandwich enzyme immunoassay kit (R&D Systems) was used to quantify the amount of VEGF secreted by the cells in the patches. The frozen media was thawed and incubated for 2 h in a well precoated with a polyclonal antibody specific for mouse VEGF, followed by incubation with an enzyme-linked polyclonal antibody specific for mouse VEGF. The color intensity of the resultant blue byproduct was measured using a microplate reader (BioTek), and the amount of VEGF was calculated from a calibration curve (Figure S5, Supporting Information).

Analysis of Angiogenesis Via CAM: The angiogenic functionality of the VEGF-secreting patches was analyzed in ovo via implantation onto a chick chorioallantoic membrane. Patches that had been incubated overnight in GM supplemented with TPA (100 ng mL^{-1}) were placed on the membranes and incubated for one week. After this period, the membrane tissue was fixed in paraffin and histological sections were stained for cell nuclei (haematoxylin) and alpha-smooth actin (α-SMA Immunohistology Kit, Sigma-Aldrich). Cross-sections were imaged using a digital pathology system (Nanozoomer, Hamamatsu) and the number and areas of blood vessels were quantified using accompanying software.

Statistical Analysis: Statistical analysis performed via one-way analysis of variance (ANOVA) followed by Tukey's Multiple Comparison Test for $P < 0.05$ using OriginPro software. Results are presented as mean ± standard deviation.

Supporting Information

Supporting Information is available from the Wiley Online Library or from the author.

Acknowledgements

The authors thank Caroline Cvetkovic for technical discussions regarding SLA. This work was funded by the National Science Foundation (NSF) Science and Technology Center: Emergent Behavior of Integrated Cellular Systems (EBICS) Grant CBET-0939511. R.R. was funded by an NSF Graduate Research Fellowship (Grant DGE-1144245) and NSF IGERT Fellowship (Grant 0965918).

Received: September 7, 2015
Revised: October 21, 2015
Published online:

[1] F. Pampaloni, E. G. Reynaud, E. H. K. Stelzer, *Nat. Rev.* **2007**, *8*, 839.
[2] D. R. Albrecht, G. H. Underhill, T. B. Wassermann, R. L. Sah, S. N. Bhatia, *Nat. Methods* **2006**, *3*, 369.

[3] M. Théry, *J. Cell Sci.* **2010**, *123*, 4201.
[4] D. Huh, B. D. Matthews, A. Mammoto, M. Montoya-Zavala, H. Y. Hsin, D. E. Ingber, *Science* **2010**, *328*, 1662.
[5] S. V. Murphy, A. Atala, *Nat. Biotechnol.* **2014**, *32*, 773.
[6] C. Cvetkovic, R. Raman, V. Chan, B. J. Williams, M. Tolish, P. Bajaj, *Proc. Natl. Acad. Sci. USA* **2014**, *111*, 10125.
[7] J. A. S. Neiman, R. Raman, V. Chan, M. G. Rhoads, M. S. B. Raredon, J. J. Velazquez, R. L. Dyer, R. Bashir, P. T. Hammond, L. G. Griffith, *Biotechnol. Bioeng.* **2015**, *112*, 777.
[8] S. M. Peltola, D. W. Grijpma, F. P. W. Melchels, M. Kellomaki, *Ann. Med.* **2008**, *40*, 268.
[9] P. Bajaj, R. M. Schweller, A. Khademhosseini, J. L. West, R. Bashir, *Annu. Rev. Biomed. Eng.* **2013**, *16*, 247.
[10] D. T. Pham, R. S. Gault, *Int. J. Mach. Tools Manuf.* **1998**, *38*, 1257.
[11] F. P. W. Melchels, J. Feijen, D. W. Grijpma, *Biomaterials* **2010**, *31*, 6121.
[12] R. Raman, R. Bashir, in *Essentials of 3D Biofabrication and Translation*, (Eds. A. Atala, J. Yoo), Academic Press, **2015**, p. 89.
[13] D. Dendukuri, S. S. Gu, D. C. Pregibon, T. A. Hatton, P. S. Doyle, *Lab Chip* **2007**, *7*, 818.
[14] U. Mirsaidov, J. Scrimgeour, W. Timp, K. Beck, M. Mir, P. Matsudaira, G. Timp, *Lab Chip* **2008**, *8*, 2174.
[15] B. Bhaduri, H. Pham, M. Mir, G. Popescu, *Opt. Lett.* **2012**, *37*, 1094.
[16] M. S. Hahn, L. J. Taite, J. J. Moon, M. C. Rowland, K. A. Ruffino, J. L. West, *Biomaterials* **2006**, *27*, 2519.
[17] C. Sun, N. X. Fang, D. M. Wu, X. Zhang, *Sens. Actuators* **2005**, *121*, 113.
[18] V. Chan, P. Zorlutuna, J. H. Jeong, H. Kong, R. Bashir, *Lab Chip* **2010**, *10*, 2062.
[19] P. Zorlutuna, J. H. Jeong, H. Kong, R. Bashir, *Adv. Funct. Mater.* **2011**, *21*, 3642.
[20] P. Bajaj, D. Marchwiany, C. Duarte, R. Bashir, *Adv. Healthcare Mater.* **2012**, *2*, 450.
[21] P. Soman, P. H. Chung, A. P. Zhang, S. Chen, *Biotechnol. Bioeng.* **2013**, *110*, 3038.
[22] S. R. Khetani, S. N. Bhatia, *Nat. Biotechnol.* **2008**, *26*, 120.
[23] C. G. Williams, A. N. Malik, T. K. Kim, P. N. Manson, J. H. Elisseeff, *Biomaterials* **2005**, *26*, 1211.
[24] S. J. Bryant, C. R. Nuttelman, K. S. Anseth, *J. Biomater. Sci., Polym. Ed.* **2012**, *11*, 439.
[25] J. Stampfl, R. Liska, in *Stereolithography: Materials, Processes and Applications* (Ed: P. J. Bártolo), Springer, Boston, MA, **2011**, 161.
[26] M. W. Tibbitt, K. S. Anseth, *Biotechnol. Bioeng.* **2009**, *103*, 655.
[27] K. Arcaute, B. K. Mann, R. B. Wicker, in *Stereolithography: Materials Processes and Applications* (Ed: P. J. Bártolo), Springer, Boston, MA, **2011**, p. 299.
[28] P. F. Jacobs, in *Rapid Prototyping and Manufacturing: Fundamentals of Stereolithography*, Society of Manufacturing Engineering, Dearborn, MI, **1992**, p. 28.
[29] J.-W. W. Choi, E. MacDonald, R. Wicker, *Int. J. Adv. Manuf. Technol.* **2009**, *49*, 543.
[30] K. Arcaute, B. Mann, R. Wicker, *Acta Biomater.* **2010**, *6*, 1047.
[31] R. Gauvin, Y.-C. C. Chen, J. W. Lee, P. Soman, P. Zorlutuna, J. W. Nichol, H. Bae, S. Chen, A. Khademhosseini, *Biomaterials* **2012**, *33*, 3824.
[32] S. P. Grogan, P. H. Chung, P. Soman, P. Chen, M. K. Lotz, S. Chen, D. D. D'Lima, *Acta Biomater.* **2013**, *9*, 7218.
[33] C. Xia, N. X. Fang, *J. Micromech. Microeng.* **2009**, *19*, 115029.
[34] H. Park, C. Cannizzaro, G. Vunjak-Novakovic, R. Langer, C. A. Vacanti, O. C. Farokhzad, *Tissue Eng.* **2007**, *13*, 1867.
[35] M. Nomi, A. Atala, P. De Coppi, S. Soker, *Mol. Aspects Med.* **2002**, *23*, 463.
[36] J. H. Jeong, V. Chan, C. Cha, P. Zorlutuna, C. Dyck, K. J. Hsia, R. Bashir, H. Kong, *Adv. Mater.* **2012**, *24*, 58.